International Journal of Advances in Engineering and Management (IJAEM)
Volume 6, Issue 10 Oct. 2024, pp: 517-528 www.ijaem.net ISSN: 2395-5252

Geological and Geophysical Delineation of Aquifers within Maikunkele and its Environs, North-Central, Nigeria

Monday Imooje[1], Sadiq Ilyasu[2,]Surajo U. Dawusu[3],Dahiru Adamu[4], Kelechi O. Rita[5], Kelechi P. Isiguzo[2]

[1]*Department of Soil Science, Federal College of Land Resources Technology, Owerri*
[2]*Department of Agricultural Engineering Technology, Federal College of Land Resources Technology, Owerri.*
[3]*Civil Engineering Department, Bayero University Kano, Nigeria*
[4]*Department of Bioenvironmental Engineering Technology, Audu Bako Coll. of Agric., Danbatta.*
[5]*Department of Science Laboratory Technology, Federal College of Land Resources Technology, Owerri.*

Date of Submission: 20-10-2024 Date of Acceptance: 30-10-2024

ABSTRACT: The delineation of aquifers in Maikunkele and its surroundings was achieved by the analysis of data from Vertical Resistivity Sounding (VES) and aeromagnetic measurements of regolith water level in hand-dug wells. The predominant rock type in the region is granite. Aeromagnetic fractures often have a 1000–2000 m length and a NE–SW trend. A handful of the cracks have a NW–SE pattern. Measurements of the water level in manually dug wells were used to create the water level map. The groundwater flow in the regolith aquifer is shown on the map to be NE–SW. This implies that there is likely an intrusion of the NE-SW cracks. Twelve stations with a maximum current electrode spacing of 200 metres carried out the VES. According to the VES data, the resistivity value of the regolith aquifer ranges from 60 to 100 Ωm, and its base extends between 10 and 40 m. Additionally, they disclosed that the 100–500 Ωm resistivity values of the fractured basement aquifer, which spans between 10 and 60 m, immediately underlies the regolith aquifer. As a result, the direction in which regolith groundwater flows can be affected by basement fissures.

KEYWORDS: Maikunkele, Delineation, aquifers, Geology, Hydrology, Geophysical Investigation.

I. INTRODUCTION

The reason basement rocks are unpredictable in terms of groundwater growth was highlighted by [5]. In Gosa, Abuja, north-central Nigeria, they therefore combined geoelectrical surveys with lineaments drawn from hill-shaded SRTM data to reduce the danger of drilling non-yielding boreholes. Interpreted two-dimensional (2D) geoelectric section results show that weathered overburden was not thick enough in several areas of the area to enable a high yielding borehole. The area's main fracture trends are NNE-SSW and N-S, which are similar to Pan-African tendencies in Nigeria's Basement Complex. Permeability of the fractured zone was facilitated by the lineaments' adequate interconnectivity. Interconnected fractures are hence the ideal structural characteristics that can raise aquifer potential. Thus, in a hydrogeologically complicated environment, our study showed the value of combining traditional vertical electrical sounding (VES) surveys with structural data from digitally altered SRTM imaging. According to [4], electrical resistivity surveys are based on measurements made on the ground surface to determine the subsurface resistivity distribution and have been utilised in hydrogeological investigations for many years. Additionally, he mentioned that groundwater investigations are now using IP and SP data. [3] used resistivity imaging in conjunction with SP techniques to locate fruitful boreholes in Sri Lanka's basement complex. They discovered that low resistivity anomalies and negative SP together suggested water-saturated fractures.

Thus, in a hydrogeologically complicated environment, our study showed the value of combining traditional vertical electrical sounding (VES) surveys with structural data from digitally altered SRTM imaging. According to [4], electrical resistivity surveys are based on measurements made on the ground surface to determine the subsurface

International Journal of Advances in Engineering and Management (IJAEM)
Volume 6, Issue 10 Oct. 2024, pp: 517-528 www.ijaem.net ISSN: 2395-5252

resistivity distribution and have been utilised in hydrogeological investigations for many years. Additionally, he mentioned that groundwater investigations are now using IP and SP data. [3] used resistivity imaging in conjunction with SP techniques to locate fruitful boreholes in Sri Lanka's basement complex. They discovered that low resistivity anomalies and negative SP together suggested water-saturated fractures.

II. MATERIALS AND METHODS

2.1 Materials

The base map (a portion of Zungeru sheet 163 SE), field notebook, digital camera, resistivity metre (McOHM Model-2115) and its accessories, global positioning system (GPS), compasse-clinometer, sample bag and geological hammer are among the materials used for this investigation. Four insulated wire clips, wooden survey pegs, four geologic hammers, two measuring tapes (100), four metal electrodes, twelve-volt batteries and extension reels are the accessories for the resistivity metre.Lithology, surface structural data, published geology and topographic maps, electromagnetic data, and vertical electrical sounding data are the primary data derived.

2.1.1 Location, Extent and Accessibility of the Study Area

The research area is located in Niger State's Bosso Local Government Area in North-Central Nigeria. It is located on Zungeru Sheet 163, towards the southeast. The geographical boundaries of the region are as follows: latitudes N9°40′00′ to N9°43′00ᶦ and longitudes E6°28′00′ to E6°30′00′ (Figure.1).There are 24 km2 covered in total. The Minna - Zungeruroad provides access to the area.

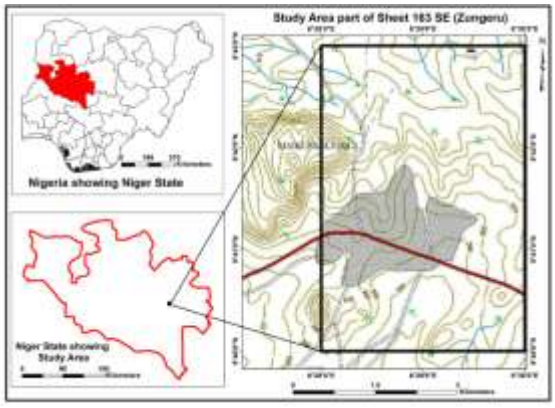

Figure1 Location of the Study Area

2.1.1 Software

Microsoft Excel, Winresist, Rock Works, Suffer 13, and Microsoft Excel are the programmes used in this study to analyse data.

2.2.0 Methodology

The methodology of the study consists of four steps:

- Desk study
- Geological field mapping,
- Vertical electrical sounding,
- Integrated interpretation of surface geological and geoelectrical data, and vertical electrical sounding

2.2.1 Desk Study

This included a thorough evaluation of the literature on the study area's geology as well as methods for acquiring and interpreting aeromagnetic and geoelectrical data.

2.2.2 Geological Field Mapping

A reconnaissance study was conducted to identify the sites of the area's hand-dug wells and boreholes. The region was then thoroughly mapped geologically using a 1:10,000 scale topographic map of Zungeru (a portion of sheet 163SE). Numerous transverse sections were examined to find outcrops. Rock lithologies were determined by taking samples of the rock. For foliated rocks, the strike and dip were measured. Utilising a compass and clinometer, the values of strike and dip magnitude were determined. A geographic positioning system (GPS) was then used to plot the results on the base map. When detected, the joints and faults were identified. Digital camera photos of joints, flaws, and outcrops were captured.

2.2.3 Vertical Electrical Sounding

Both the town's centre and the nearby farmlands on the outskirts underwent vertical electrical sounding. This will make it simple to access any boreholes that may later be found thanks to the study's findings. Eight transverses, each 100 metres apart, were used for the sounding. The electrodes were extended (moved) along the strike, and the transverse were arranged along the dip directions. Along the dip- ways, the transverse lines marked the locations of the sounding stations. While the strike direction is N-S, the dip direction is eastward.

The distance between the sounding stations was 100m. The Schlumberger electrode array (Figure 3) geoelectric metre was used for the sounding. A 200 m maximum electrode separation was employed. The resistance (R) recorded in metre was translated into apparent resistivity **ρ**a using,

International Journal of Advances in Engineering and Management (IJAEM)
Volume 6, Issue 10 Oct. 2024, pp: 517-528 www.ijaem.net ISSN: 2395-5252

$\rho a = [(AB/2)^2 - (MN/2)^2] \times R$……..……1
MN/2

The
$[(AB/2)^2 - (MN/2)^2]$.....2
(MN/2)
Where AB is current electrode spacing, MN is potential electrode spacing.

Equation 11 contains a geometric component. The values of AB, MN, and G used to calculate **ρ**a from R.

At each location, the **ρ**a values were plotted on a log-log graph.A mixture of eyeballing, recognised values of soil and weathered basement thickness, cumulative **ρ**a versus AB/2 plot, and reconnaissance were used to derive the geoelectric section model. Win-resist was employed in the modelling of the theoretical geoelectric section. Up until a fit was achieved, the theoretical model and the inferred model were interactively changed. Every sounding station's elevation and geographic coordinates were recorded using the GPS. To determine the sub-sea depth to each geoelectric layer, the depth to the top of each layer (obtained from the geoelectric sections) was deducted from the station elevation. Apparent resistivity map, thickness map, sub-sea depth to top map was generated for regolith interval, and confined fracture intervals. Transverse unit resistance (Ti) was estimated for regolith and confined fracture intervals using equations using equation 12Ti = $\sum_{i=n}^{n} \rho i * hi$.....3
Where hi and **ρ**i are the thickness and apparent resistivity of thegeoelectric intervals. Using surfer 13, **ρ**a, thickness, Ti values were contoured for regolith, first and second confined fracture intervals.

Plate I:McOHM Resistivity Meter Model-2115

2.2.4 Geo-electric Sections

To make it easier to compare the geoelectric properties of the subsurface variation, geo-electric sections spanning VES locations in the basement portion of the study region were obtained. They display several resistivity-based geo-electric layers found in the subsoil. Each layer's depth is displayed, making it possible to determine the extent of each layer and its distance from newly formed rock with clarity. To create a close picture of the subsurface layers, the resistivity of the different layers is assigned to their corresponding depths, and zones with the same geo-electric signatures are joined. This yields the geo-electric section. Logs from previously drilled boreholes and hand-dug wells were used as controls in this process. Three separate layers are identified by the geo-electric sections along the traverses in the research area: the fresh basement, the weathered/fracture zone, and the topsoil.

2.3 Processing of Aeromagnetic Data

Fugro Airborne Surveys Limited, a Canadian company, conducted the aerial magnetic geophysical research. A proton precession magnetometer with a precision of 0.01nT was used to collect the aeromagnetic data, which were collected along a sequence of NE-SW tie lines with a 500 m flight line spacing and an 80 m terrain clearance. Using the coordinates of the vertices in the Oasis Montaj programme, the micro-leveled magnetic data encompassing the research region was windowed out. The minimum curvature gridding approach [1] was used to grid the data. The super-regional field of 32000nT was subtracted from the raw data, and the total magnetic intensity field was corrected using the IGRF (International Geomagnetic Reference Field, 2009). To position the anomalies vertically above their sources, the Reduction to Equator (RTE) approach was used. While the depth analysis technique assisted in the quantitative understanding of the underlying magnetic anomalies, the filtering process helped with the qualitative interpretation of the abnormalities. To precisely place anomalies right above their causal bodies, RTE was used to the collected aeromagnetic data. The RTE procedure was conducted at the central position of the study region, which has a geomagnetic declination and inclination of -2.03° and -4.73°, respectively.

2.3.1 First Vertical Derivative (FVD).

The data's first vertical derivative was calculated to facilitate the identification of lines. In the research area, shallow anomalies are better suited for groundwater exploration, whereas deeper abnormalities are suppressed by this procedure. Although higher order derivatives are linked to noise that renders interpretations useless, the second vertical derivative pursues this effect even farther.

International Journal of Advances in Engineering and Management (IJAEM)
Volume 6, Issue 10 Oct. 2024, pp: 517-528 www.ijaem.net ISSN: 2395-5252

The equation of the wavenumber domain filter to produce nth derivative is:

$$F(\omega) = \omega^n \quad 4$$

Where: F = vertical derivative
ω = wavenumber (radians/ground unit)
n = order of differentiation
Note: $\omega = 2\pi k$ where k is cycles/ground unit.

2.3.2 Tilt Derivative

The TDR filter was used to both the RMI and the RTP grid in order to identify structures (fault and folds), contacts, edges, and boundaries of magnetic sources, as well as to increase weak and strong magnetic anomalies of the region. By placing an anomaly exactly over its source, the tilt angle derivative filter aims to locate it. The tilt derivative filter is an automatic-gain-control (AGC) filter that tends to equalise the response from both weak and strong anomalies, as demonstrated by [9]. This makes it a useful tool for tracing out along striking abnormalities. The hypothesis that the zero contours are the edges of the formation is used by the tilt angle derivative (TDR) of RMI to detect the edges of formations, particularly at shallow depths. [8].

2.3.3 Analytic Signal (AS)

The three orthogonal derivatives of the analytical signal of the total magnetic field T are used to compute the amplitude A, as shown by [7].

$$A(X,Y)| = \sqrt{\left(\frac{\partial_1}{\partial x}\right)^2 + \left(\frac{\partial_1}{\partial y}\right)^2 + \left(\frac{\partial_1}{\partial z}\right)^2} \quad 5$$

Where A = amplitude of the analytic signal
T = total magnetic field
x, y and z = orthogonal directions

By using finite differences to determine the total intensity magnetic anomaly field derived from Singh and Sabina's formulas (1978), the modelled grid of analytic signal was produced. The magnetic field's vertical derivative was calculated for depths of (z + x) and (z - x) by dividing the difference between the depths by 2x. The same formula is used to determine the derivatives of x and y. On the other hand, analytic signal connections are frequently more irregular than their horizontal derivative. The edge of magnetization is exactly proportional to the magnitude of the analytic signal peak. Therefore, determining source edges is simple.

2.4 Lineament Mapping, Analysis and Interpretation

This project's methodology was akin to that of [7], who employed four main processes in lineament analysis:

i) Lineament data acquisition from different datasets
ii) Lineament analysis to identify significant data
iii) Presentation of results as statistical and spatial plots
iv) Comparison of lineaments with fracture data acquired from the field.

Visual inspection was used to identify the lineaments, which were then interactively digitalized in the pictures. Based on the entire body of information gathered from the digital augmentation of individual single band and composite photos as well as ground truth data, a lineament map was created. For every dataset, a separate lineament mapping was completed.

Roads and railroads were among the auxiliary data that were presented alongside each dataset when it was imported into an ArcGIS 10.3 project. To make sure that manmade features weren't incorrectly classified as a structurally-related lineament, the supplementary data were superimposed on the map. This has disadvantages in that it could lead to the incorrect exclusion of geological formations that overlap with anthropogenic features. A geodatabase was made in ArcCatalog to hold the digitised lineaments as polylines together with related lineament data such the length, orientation, and category. A digitised line segment had to be at least one kilometre long.

2.4.1 Lineament Extraction from Aeromagnetic Data

Using the computer's mouse, the lineaments were extracted from the shaded relief image of the tilt derivative, FVD, and total intensity magnetic anomaly maps through visual inspection on the screen. By visually examining the various geophysical map versions at various sizes and digitising the orientation of each interpreted lineament, the qualitative interpretation of the lineaments was completed. The magnetic total field map served as both the foundation for the interpretation and the most significant collection of data. The displacements and discontinuities of magnetic anomalies, together with all zones of magnetic minima, were digitalized. The magnetic lineaments were then added as a separate layer and superimposed. Some lines may not appear precisely where they would have if they had been drawn on a smaller scale map and digitised due to parallax

International Journal of Advances in Engineering and Management (IJAEM)
Volume 6, Issue 10 Oct. 2024, pp: 517-528 www.ijaem.net ISSN: 2395-5252

effects on the on-screen view. Visually evident patterns were drawn on the screen; while efforts were made to cover all trends one kilometre or longer, some were undoubtedly missed, especially those that ran approximately parallel to a neighbouring trend that had already been drawn.

2.4.2 Lineament Analysis

The length and total number of the lineaments served as the basis for the statistical analysis of the lineaments in the current study. Analysis was also done on the lineaments' maximum, lowest, and average lengths as well as their standard deviation. To display the lineaments' orientation distribution, rose diagram analyses were produced. Rose diagrams were created using software tools from Rockworks 16 (RockWare).

III. RESULTS AND DISCUSSIONS

3.1 Field Geology

Granite is the type of rock that is exposed at Maikunkele and the surrounding area (Plate I). Figure 2 shows the geographical and structural link between these outcrops, with the rocks trending NNE-SSW. Joint fractures are a common occurrence on the outcrops. Plate II shows that there are three sets of joints: oblique, dip, and strike joints. While the dip joints trend along dip, the strike joints trend along strike. The oblique joints follow a diagonal tendency in the direction of strike and dip. The measured joint direction values are shown in Table 4. While some of the Joints are devoid of mineralization, others (Plate III) are rich in quartz. NNE – SSW is the primary joint direction shown by the Joints' Rossette diagram plot (Figure 4.1).

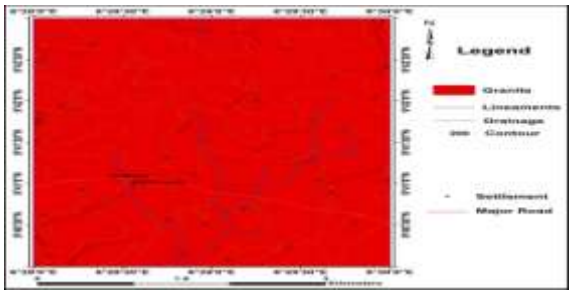

Figure 2 Geological map of the study area

Plate II: Granite $9^0 40' 28'' N - 6^0 29' 59'' E$

Plate III: Quartzite intrusion $9^0 41' 12'' N - 6^0 28' 10'' E$

Plate IV:Joint $9^0 40' 27'' N - 6^0 28' 11''E$

LOCATION	LONGITUDE	LATITUDE	ELEVATION	STATIC W/L	HYDROLIC HEAD
W1	$006^0$29'02"E	$09^0$41'24"N	292	2.3	289.7
W2	$006^0$29'02"E	$09^0$41'23"N	334	1.5	332.5
W3	$006^0$29'05"E	$09^0$41'23"N	303	1.3	301.7
W4	$006^0$28'09"E	$09^0$40'59"N	299	2.0	297

International Journal of Advances in Engineering and Management (IJAEM)
Volume 6, Issue 10 Oct. 2024, pp: 517-528 www.ijaem.net ISSN: 2395-5252

W5	006^{0}28'09"E	09^{0}40'24"N	248	1.1	246.9
W6	006^{0}28'58"E	09^{0}41'05"N	280	3.2	276.8
W7	006^{0}28'03"E	09^{0}41'10"N	302	1.7	300.3
W8	006^{0}29'10"E	09^{0}41'24"N	289	2.5	286.5
W9	006^{0}29'12"E	09^{0}41'55"N	308	2.8	305.2
W10	006^{0}29'15"E	09^{0}41'20"N	282	2.4	279.6
W11	006^{0}29'57"E	09^{0}40'51"N	290	1.6	288.4
W12	006^{0}28'50"E	09^{0}40'09"N	285	2.1	282.9
W13	006^{0}28'45"E	09^{0}41'30"N	291	1.5	289.5
W14	006^{0}28'40"E	09^{0}40'56"N	282	2.8	279.2

Plate VI: Well inventory measurement (006°29´10´´E and 09°41´24´´N)

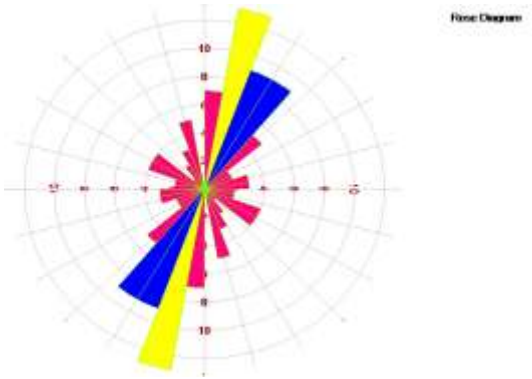

Figure 3: Rossette Diagram of joints in the study area.

3.2 Hydrogeological mapping

One of the techniques used to investigate the groundwater in the region was hydrogeological mapping. The studied wells yielded static water levels ranging from 1.1 m to 2.8 m (Table 2). data was utilised to create a vector map with surfer to show potential paths of groundwater movement. According to the groundwater flow direction map (Figure 3), the flow is primarily in the southwest direction.

International Journal of Advances in Engineering and Management (IJAEM)
Volume 6, Issue 10 Oct. 2024, pp: 517-528 www.ijaem.net ISSN: 2395-5252

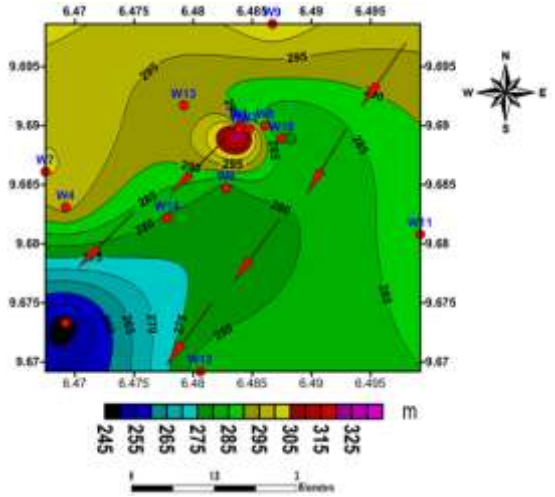

Figure 4: Groundwater flow map showing direction of flow

Geophysical investigation interpretations

3.3.1 Description of Curves

In order to estimate the depths and resistivity of the strata present, Vertical Electrical Sounding (VES) was used in the research region to determine how resistivity varies with depth below a given spot on the ground surface and to correlate it with the existing geological information.Figure 5a-b, the Electrical Sounding Curves result, displays the HA and A curve types; appendix 3 lists additional curve types in the study area. The basement area's curves almost entirely depict a three-layer structure (Figure 5a–b). The top soil layer, the worn/fractured layer, and the newly formed basement are among the layers. Lateritic clay and sandy, clayey sand with resistivities ranging from 18.9 Ωm to 567 Ωm make up the top layer. The top soil layer has a thickness ranging from 1.3 to 4.4 metres. The second layer of geo-electricity is the weathered/fractured layer, with resistivity ranging from 6.7Ωm to 452.6Ωm. This layer ranges in thickness from 4.2 to 35.8 metres. At 35.8 metres, VES 05 has the thickest layer, and at 4.2 metres, VES 06 has the thinnest. At 9202.9Ωm, fresh basement rock exhibits a high resistivity value.

Important conclusions have been drawn from a thorough examination of the several outcomes of the methods used to evaluate the study's groundwater potential. The composition and saturation of the top soil account for the variation in resistivity values of the VES curves, particularly for the upper soil layers. When developing groundwater, hydrogeological factors such as topsoil thickness are crucial. This is because the top soil layer allows water to enter the saturated zone. The intermediate layers are equally crucial. There is a considerable chance of finding good groundwater storage in this zone, which is the worn and/or fractured layer. Generally, thicknesses more than 10 m are favoured. In every station, the new basement is composed of infinitely resistive rock. The bedrock is formed by it. This zone is not a water-bearing zone because the rocks there are hard and impervious.

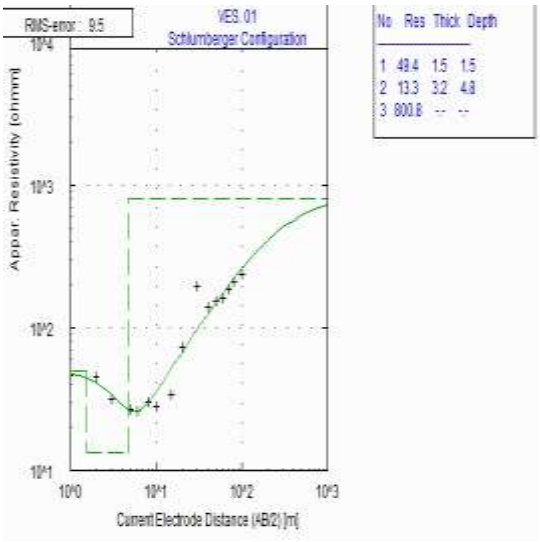

Figure 5a: A typical HA – type

International Journal of Advances in Engineering and Management (IJAEM)
Volume 6, Issue 10 Oct. 2024, pp: 517-528 www.ijaem.net ISSN: 2395-5252

AB/2	MN/2	G	R	ρa
1	0.5	2.36	148.06	349.43
2	0.5	11.8	29.31	345.87
3	0.5	27.5	4.720	129.81
5	0.5	77.8	3.197	248.69
6	0.5	112	2.075	232.35
6	1.0	55	4.622	254.19
8	1.0	99	2.758	273.09
10	1.0	156	2.313	360.85
10	2.50	58.9	5.196	306.00
15	2.5	137	3.205	439.09
20	2.5	247	2.633	650.45
30	2.5	562	1.241	697.20
40	2.5	1001	0.654	655.08
40	7.5	323	2.102	678.85
50	7.5	512	1.328	749.74
60	7.5	742	1.265	938.74
70	7.5	1015	1.156	1173.5
80	7.5	989.73	1.328	1354.7
80	15	647	1.939	1254

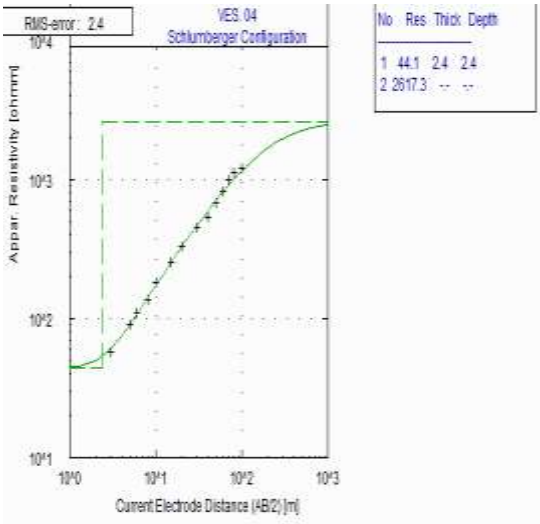

Figure 5b: A typical A – type curve

International Journal of Advances in Engineering and Management (IJAEM)
Volume 6, Issue 10 Oct. 2024, pp: 517-528 www.ijaem.net ISSN: 2395-5252

3.3.2 Isopach Map (Depth to Bedrock) of Maikunkele and its environs

The entire research region has had varied degrees of weathering, and the basement has experienced significant fracturing, according to the isopach map of depth to the basement (Figure 4). The most heavily weathered areas are in the south western and south eastern sections of the region; the middle portion of the area, particularly in profile C, and a small fraction of the south western area were determined to be minimally weathered. According to [10], heavy bedrock overburden is a sign of likely rock fracturing because thicker regolith puts greater strain on the rock and increases the likelihood of rock fracturing. Another sign that the bedrock is likely to fracture is low resistivity.

3.3.3 Iso-resistivity Map of Maikunkele and its environs.

To conduct a comprehensive analysis of the resistivity's continuous fluctuation with depth, iso-resistivity maps were created at 20 and 80 metres below the surface. These maps provide a thorough and in-depth analysis of the hydro-geophysical aspects of the research region. Relatively good conductors and places with groundwater potential are found in areas with low resistivity values, whilst poor conductors and poor groundwater potentials are found in areas with high values. The northwest and northeastern regions of this area are indicated by high resistivity. Lower resistivity in the southwest and southeast of the region indicates a location with good groundwater potential and rock unit fracturing.

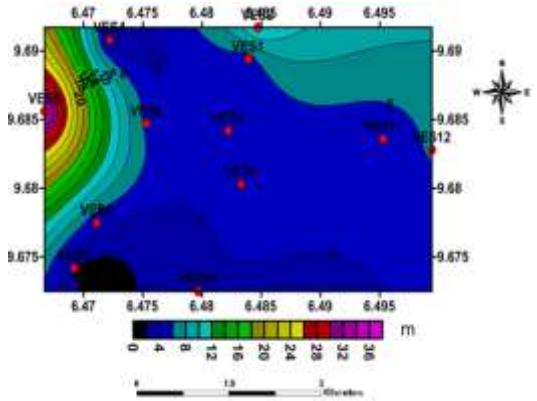

Figure 6 Isopach Map of Maikunkele and its environs

Groundwater flow is favoured southward by the geography of the basement. A location of ground water collecting is located in the southeast. The south of the study area has a large area of deep basement, whereas the central portion along the north-west line is shallow. As a result, groundwater flows away from the central portion, preferably to the south or south-east.

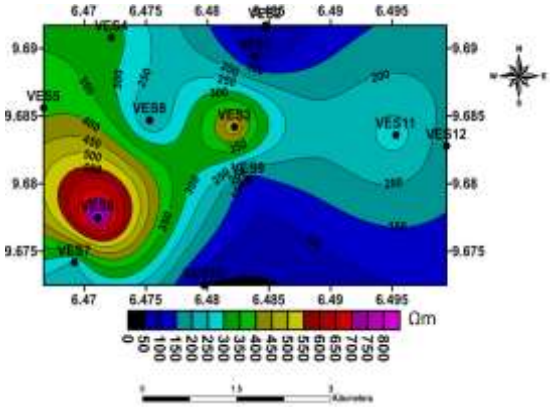

Figure 7 Isoresistivity Map of Maikunkele and its environs At 20m

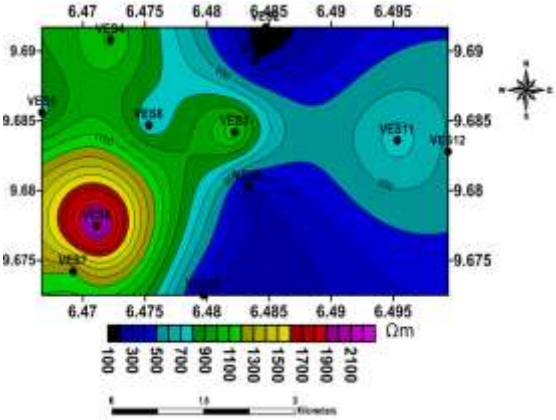

Figure 8 : Iso resistivity map of Maikunkele and its environs at 80m

3.3.4 Geo-electric Sections of the study area

Three geo-electric layers comprise the geo-electric sections of the VES 3, 5, 8, 11, and VES 6, 9, 12. The topsoil's resistivity ranges from 45 m to 237 m, and it is primarily made of clay, laterites, and lateritic clay. The zone is where surface water infiltrates and evaporates; the large range of resistivity fluctuation is caused, among other things, by variations in the degree of compaction and lateralization. The resistivity range of the second layer, which lies directly beneath the topsoil and is depth to the weathered foundation layer, is 34 m to 1870 m. Feldspar, a byproduct of the basement granitic rock's weathering, is the main mineral found in the rocks in this zone. Because of its higher porosity and permeability than the top soil layer above, this layer has a lower resistivity value.

The permeability and porosity of this zone play a crucial role in the occurrence and storage of

International Journal of Advances in Engineering and Management (IJAEM)
Volume 6, Issue 10 Oct. 2024, pp: 517-528 www.ijaem.net ISSN: 2395-5252

groundwater in this area. When it has a noticeable thickness, this zone is typically used as the primary target unit for locating sustainable groundwater boreholes. The cracked zone, which is immediately below the worn layer, is the following layer. The resistivity values of the layer vary from 1Ωm to 289Ωm. The layer's thickness and resistivity vary as a result of variations in the degree of fracturing and the weathering that follows. Given its secondary permeability, this zone has the capacity to store large amounts of groundwater and significantly enhance the weathered layer above. The fresh basement, which makes up the third layer, has a resistivity of up to 2122 m, is infinitely thick, and is nearly completely porous, making it difficult for groundwater to accumulate or store. One may argue that the fresh basement provides the necessary mechanical support for all the overlaying sequences known as the top soil, weathered/fractured basement, as all the other layers depend on this layer.

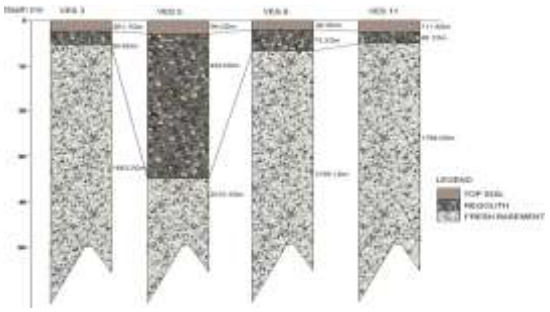

Figure 9 Geo-electric Section for VES 3, 5, 8 and 11.

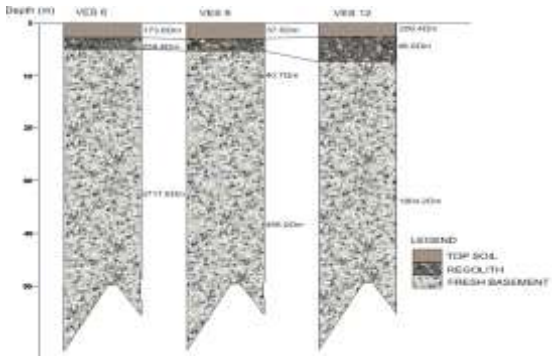

Figure 10 Geo-electric Section for VES 6, 9 and 12.

3.4 Lineament Extracted from Aeromagnetic map

The aeromagnetic map's recovered lineaments are mostly orientated in the NNE–SSW directions (Figure 8). These lineament directions show good agreement with surface-mapped joint directions (Figure 6). Additionally, the NE-SW trending structures are aligned to the Pan-African regional tectonics, suggesting a sort of structural control over the drainage system. These lineaments also correspond to the alignment of stream segments.

Mylonites in the area have attributed a NE–SW trend to this deformation event, which is strongly linked to the creation of the schist belts.

3.5 Results of the Analysis of Aeromagnetic Data

3.5.1 Qualitative Analysis of the Total Magnetic Intensity Map

Figure 10 shows the total magnetic intensity anomaly map (TMI) of the research area. The residual TMI map's colour values range from blue at low to magenta at high. Values for residual magnetic intensity fall between -107 and 146.4 nT. High and low magnetic anomalies with a NE-SW trend predominate in the studied region. The magnetic anomalies in the region trend in the same direction as the surface joint system and regional geological features (lineaments) when compared to the geological map of the area. The high magnetic anomalies are indicative of the granitic rocks, according to a comparison between these anomalies and the research area's geology map.

International Journal of Advances in Engineering and Management (IJAEM)
Volume 6, Issue 10 Oct. 2024, pp: 517-528 www.ijaem.net ISSN: 2395-5252

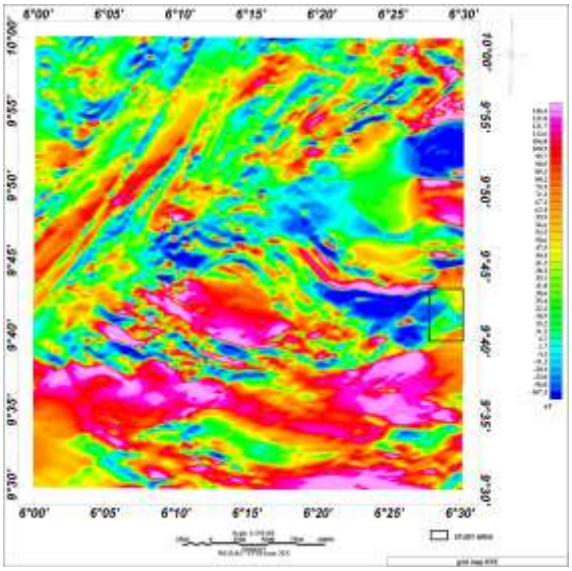

Figure 11: Total Magnetic Intensity map of Sheet 163 (Zungeru)

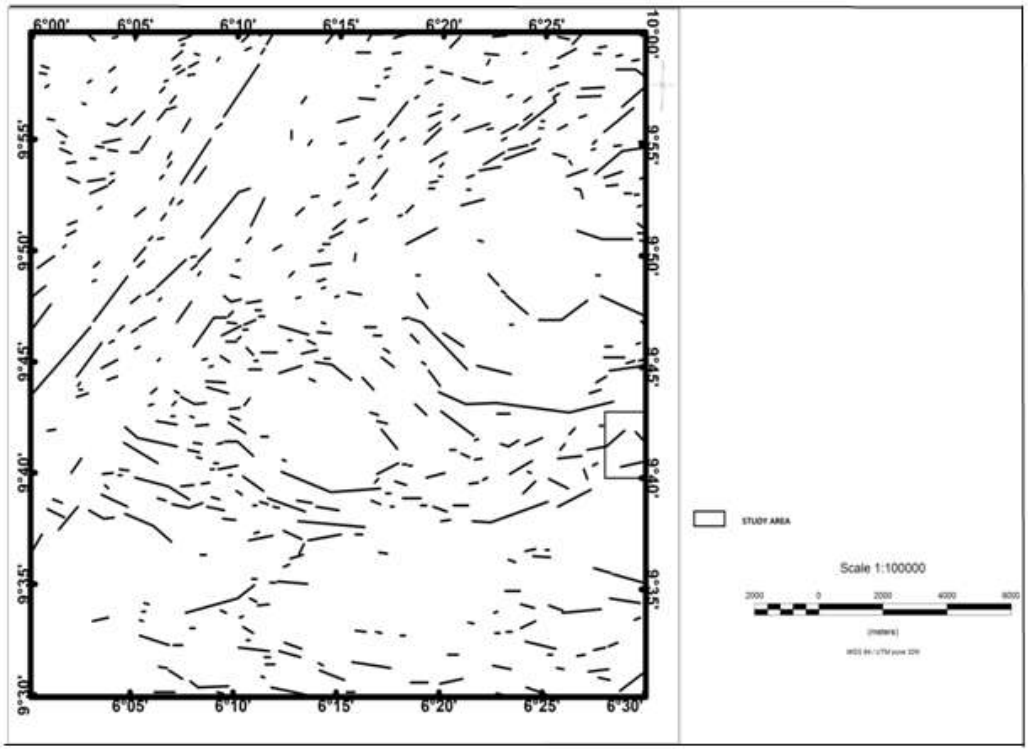

Figure 12: Lineament map developed from Aeromagnetic map.

IV. CONCLUSION AND RECOMMENDATION

4.1 Conclusion

This study found that methods such as electrical resistivity and aeromagnetic resistivity were effective in identifying the aquifer in Maikunkele and its surroundings. The fractures are represented by lineament that ranges in length from 700 to 900 metres on the magnetic lineament map. The region is characterised by granitic topography, with a predominately NNE–SW fracture trend. This appears to have an impact on the regolith aquifer's SSW water flow direction. The fractured basement aquifers in VES 1, 2, 3, 5, 9, and 12 have resistivity ranges of 65 to 760 Ωm and are located between 35 and 50 m; 80 and 100 m depth intervals.In the research area, the average regolith thickness is 7.6 metres. Because of their thicker regolith and lower

resistivity, VES 1, 2, 3, 5, 8, 9, 10, and 12 were found to have high groundwater potential by the geophysical study conducted in the study region.

Conclusively, the research area's water-yielding fractured basement aquifers are located between 35 and 50 metres and 80 and 100 metres below the surface.

4.2 Recommendations

The potential unfailing aquifers in Maikunkele and its surroundings have been identified by this research, and these findings can serve as a guide when selecting locations for the development of groundwater resources. Therefore, it is advised that;

1. Drilling can be contemplated at the following VES points where aquifers with the capacity for constant water flow exist: VES 1, 2, 4, 5, 9, 10, 11, and 12 for wells excavated by hand and boreholes pumped by hand.
2. In the SW section of the research region, motorised boreholes should be drilled into the convergence zone.
3. For a year-round supply of drinkable water in the research region, boreholes should be sunk down to a depth of more than 100 metres in locations where lineaments are seen.

REFERENCES

[1]. Briggs, I. C. (1974). Machine contouring using minimum curvature. Geophysics, 39(1), 39-48.

[2]. Jamaluddeen, S. S., Bunawa, A.A., &Saleh, M. (2014).An assessment of groundwaterpotential of Bayero University, Kano, permanent site using induced polarisation and selfpotential methods. Journal of Earth Science and Engineeering,4, 587-596.

[3]. Jinadasa, S.U.P., &DSilva, R. P. (2009). Resistivity imaging and self-potential applications in groundwater investigation in hard crystalline rocks. Journal of National Sciences Foundation, Sri Lanka37(1), 28-32.

[4]. Kumar, D., Rao, V. A., &Sarma, V. S. (2014).Hydrogeological & geophysical study for deeper groundwater resources in quartzitic hard rock ridge region from 2Dresistivity data. Journal Earth System Sceince, 123 (3), 531-543.

[5]. Maxwell, O., Wagiran, H., Ibrahim, N., Andrew, O. I., Solomon, O. O., Sabri, S.D. (2014). Integrated geoelectrical and structural studies for ground-water investigation in parts of Abuja, North Central Nigeria. Near Surface Geophysics. 12(4), 515-521.

[6]. Menkpa,E.L.A., Nouck, P.N., Atangana, J.Q. Y., &Ondona, J.M.(2015). Combineduse of electricsl and flow parameters for hydrogeological characterisation

[7]. Roest, W.R., Verhoef, I. & Pilkington, M. (1992). Magnetic interpretation using the 3-D analytic signal. Geophysics, 57(1), 116 125.

[8]. Salem, A. Simon, W. Fairhead, D. Ravat, D, Richard, S. (2007). Tilt depth method: Asimple depth estimation using first-order magnetic derivatives. The leading-edge, 26, 12

[9]. Verduzco, B. Fairhead, J.D. Green, C.M. and MacKenzie,C. (2004). New insights into magnetic derivatives for structural mapping: The leading Edge, 23, 116-119

[10]. Zohdy, A. A.,Eaton, G.P.&Mabey, D.R. (1974). Application of Surface Geophysics to Groundwater Investigation. Techniques of water resources investigations of the US Geological Survey, 2, 5-66